The Journal of The Textile Institute

ISSN: 0040-5000 (Print) 1754-2340 (Online) Journal homepage: https://www.tandfonline.com/loi/tjti20

Dynamic analysis of spinning triangle geometry part 1: validation of methodology

Noman Haleem, Stuart Gordon, Xin Liu, Christopher Hurren & Xungai Wang

To cite this article: Noman Haleem, Stuart Gordon, Xin Liu, Christopher Hurren & Xungai Wang (2019) Dynamic analysis of spinning triangle geometry part 1: validation of methodology, The Journal of The Textile Institute, 110:5, 660-670, DOI: 10.1080/00405000.2018.1511223

To link to this article: https://doi.org/10.1080/00405000.2018.1511223

Published online: 10 Nov 2018.

THE JOURNAL OF THE TEXTILE INSTITUTE
2019, VOL. 110, NO. 5, 660–670
https://doi.org/10.1080/00405000.2018.1511223

Taylor & Francis
Taylor & Francis Group

Dynamic analysis of spinning triangle geometry part 1: validation of methodology

Noman Haleem[a], Stuart Gordon[b], Xin Liu[a], Christopher Hurren[a] and Xungai Wang[a]

[a]Institute for Frontier Materials, Deakin University, Geelong, Australia; [b]CSIRO Manufacturing, Deakin University, Geelong, Australia

ABSTRACT

The physical shape or geometry of the spinning triangle directly affects the quality of ring spun yarns. This study developed a technique to measure the geometrical parameters of the spinning triangle during ring spinning using a combination of a clear rubber roller and digital image processing. The clear roller exposed the spinning triangle zone during the yarn spinning process in a non-invasive manner, and yarn properties were not affected. A digital camera recorded images of the spinning triangle. An image processing algorithm was then developed to process the images to measure the dynamic geometry of the spinning triangle. The method was able to effectively measure the width, height and skew of the spinning triangle along with changes in these parameters over time. This technique will be applied in a follow-up study to investigate the effects of the shape of the spinning triangle on yarn quality.

ARTICLE HISTORY
Received 11 February 2018
Accepted 8 August 2018

KEYWORDS
Spinning triangle; ring spinning; clear roller; image processing; yarn quality

Introduction

The critical role of the spinning triangle in determining ring yarn quality has been acknowledged frequently in research on short and long staple ring spinning (Klein, 2008; Lawrence, 2010; Mahdiyeh & Esfandiyar, 2014). There are several examples where variations in the width or angles of the spinning triangle affected yarn hairiness, uniformity, strength and elongation (Lawrence, 2010; Xia & Xu, 2013). Notable cases include compact and diagonal offset spinning, where compacting the base and offsetting the tip of the spinning triangle, respectively, achieved marked improvements in yarn quality (Altas & Kadoglu, 2012; Basal & Oxenham, 2006; Thilagavathi, Udayakumar, Sasikala, & Kannaian, 2009; Tyagi, Bhowmick, Bhattacharyya, & Kumar, 2010; Wang & Chang, 2003). Hence, a strong relationship between the spinning triangle and resultant yarn quality is understood but surprisingly its exact influence is unknown. A clearer understanding of this relationship would lead to better management and engineering around the spinning triangle and the production of superior quality yarns in a simpler and more cost effective manner. The difficulty in quantifying the spinning triangle in terms of geometrical parameters makes current understanding of the 'meagre and unsatisfactory kind', as termed by Lord Kelvin (Sears, Zemansky, & Young, 1976).

In ring spinning, the spinning triangle is formed at the nip line of the drafting rollers and the yarn twist point. In this small space, where a continuous strand of fibres is twisted into a yarn, perhaps the most useful and practically quantifiable information is the physical geometry or shape of the spinning triangle. However, there are some challenges associated with its measurement. For example, the curvature of the drafting rollers, the rapidly changing shape due to material and process related variations, the small dimensions and the fragile fibrous structure of the spinning triangle do not allow a direct and clear observation. In the past, two different approaches were applied to the study of the spinning triangle. In one approach, a lipstick type camera was mounted (in machine direction) at the delivery end of the drafting zone to record images of the spinning triangle zone (Wang, Huang, & Huang, 1999). As the base of triangle was hidden between drafting rollers, only its partial view was achieved that did not allow accurate measurement of its geometry.

In a second approach, the original top drafting roller (made up of rubber) was replaced by a clear roller (made up of plastic) and the bottom roller was covered with a rubber layer for nip formation (Feng, Xu, Tao, & Hua, 2010; Najar, 1996). Although the clear roller provided a full view of the spinning triangle, two significant issues were associated with this method. First, the rigid plastic roller did not form an adequate nip with the bottom roller. The additional rubber layer applied on the bottom roller to facilitate nip formation also covered its grooved profile, which caused poor control on the fibrous strand leading to roller slippage and excessive end breakages. Ideally, 'the fibres passing through the nip of a pair of rollers should be held firmly so that they have no motion other than that dictated by the rollers' (Lord & Grover, 1993). Second, the imagery data acquired through the clear roller for measurement of spinning triangle geometry were limited to one or a few static images (Wei, Huang, Zhu, & Su, 2015). It is important to

CONTACT Xungai Wang xungai.wang@deakin.edu.au Deakin University, Institute for Frontier Materials, Geelong, Australia.

understand that the geometry of spinning triangle continuously fluctuates under influence of various material and process related variations. Hence, a series of continuous images is required to sample and average the true geometry of the rapidly varying spinning triangle (Kennedy & Neville, 1986).

Based on the above discussion, the fundamental requirements of an eligible system to study the spinning triangle are proposed, i.e. ability to provide a complete and clear view of the spinning triangle, non-invasive operation and measurement of physical geometry of the spinning triangle by considering its dynamic nature. The first part of this study introduces a new combined method based on two components to study the spinning triangle geometry in alignment with the above-mentioned criteria. The first component consists of a newly developed clear rubber roller made up of a two layered composite structure. The roller simply clips in the drafting arm of the ring frame without requiring any further modifications and exposes the spinning triangle to an image acquisition setup. The second component consists of an image processing based system that analyses the serial images acquired in the first phase and measures the dynamic geometry of the spinning triangle in terms of suitable parameters. The purpose to develop this method is to measure the geometry of the spinning triangle in a controlled yarn spinning arrangement to establish its relationships with different yarn quality parameters, which will be discussed in the second part of this study.

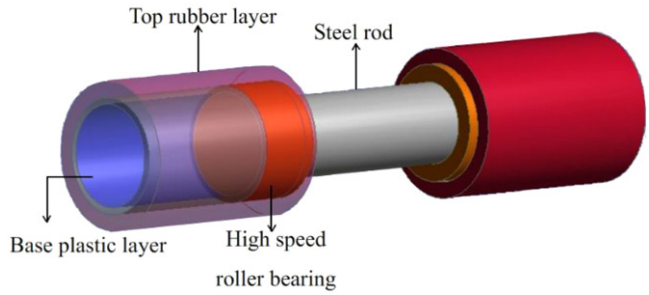

Figure 1. Composite two layered structure of the clear rubber roller.

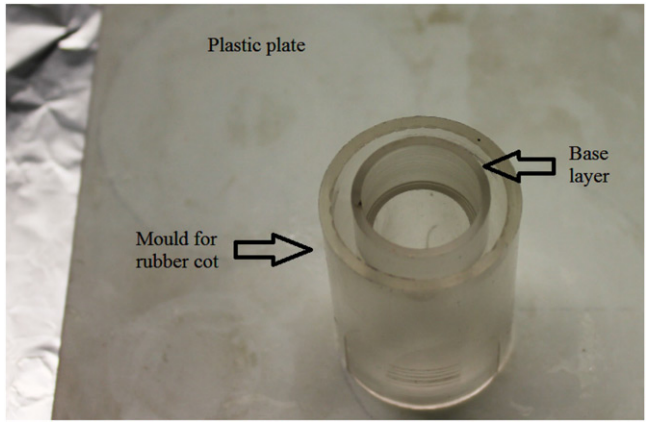

Figure 2. Concentric set of plastic tube and mould before addition of polyurethane rubber layer.

Materials and methods

Development of clear rubber roller

A clear rubber roller was developed to replace the original top roller in the drafting zone to expose the spinning triangle. The clear rubber roller possessed a composite structure as shown in Figure 1. The base layer was made up of a clear acrylic tube (16 mm ID/22 mm OD) while the top layer was formed by casting Clear Flex 95 (Smooth-on, Macungie, PA, USA), a clear polyurethane resin, around it. The hardness of the cured polyurethane rubber was 90–95 A shore, comparable to the hardness of a similar top drafting roller. The rigid base layer provided essential strength and form to the roller while the top rubber layer made an effective nip with the bottom drafting roller.

For resin casting process, a circular mould was developed from a machined acrylic tube (27.5 mm ID/32 mm OD). An aerosol-based universal mould release agent (Smooth-on, Macungie, PA, USA) was applied inside the mould to enable easy extraction of the rubber cot after curing. The base tube and mould (for the rubber cot) were fixed on a plastic plate in a concentric arrangement in order to pour the resin into the rubber cots as shown in Figure 2. The Clear flex 95, a two-part based resin system, was used at a mix ratio of 1:1.5 (by weight) of part A and part B, respectively. The resin processing was initiated by separately degassing 10 g of part A and 15 g of part B. The degassing was carried out for 10 min for each part in a vacuum chamber at negative pressure of 15 inches of mercury. After degassing separately, both parts were thoroughly mixed with each other and degassed again for 15 min to remove any air bubbles out of the mixture. The complete removal of air bubbles was critical to achieve the desired level of clarity in the roller.

The degassed resin mixture was then injected into the fine spacing between the base tube and the mould using a syringe. The resin mixture was allowed to cure in air for 18 h at 20 °C temperature. Post curing was then conducted at 70 °C for another 18 h in a laboratory oven (GE182171, Crown Scientific, Minto, NSW, Australia). Two units of clear rubber roller pieces were developed through the above mentioned process. One end of the base tube in each unit was machined on a Lathe to create a slot for mounting the outer ring (19 mm diameter) of a high-speed IKO roller bearing (IKO International, Inc., Parsippany, NJ, USA). The inner rings of the bearings were fixed on both ends of a steel rod to mount the clear rubber rollers on each side. The steel rod was also machined in its centre to clip it inside the drafting arm of the ring spinning frame. The final developed form of the clear rubber roller is shown in Figure 3.

Yarn spinning and testing

In order to test the performance of the clear rubber roller in terms of revealing the complete spinning triangle with acceptable clarity and non-invasive nature of its operation, 20 tex yarns with 798 tpm were produced from 100% cotton rovings (from 30.55 mm upper half mean length and 4.98 Micronaire cotton). The yarn spinning was conducted on an industrial scale Zinser 350 ring frame (Saurer, Wattwil, Switzerland) using the clear rubber roller. Yarns of the same

Figure 3. The clear rubber roller and original top drafting roller.

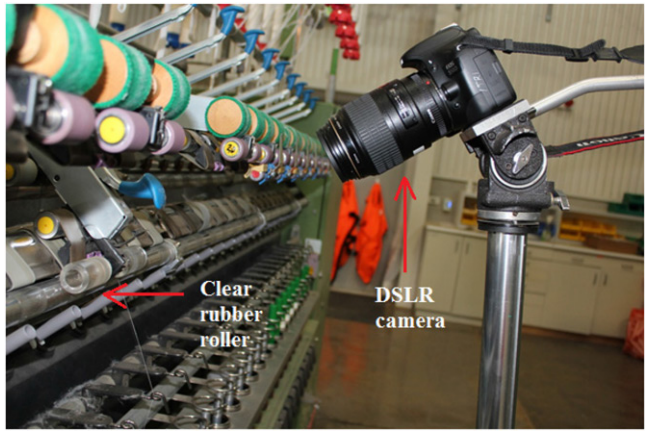

Figure 4. Image acquisition setup for recording spinning triangle geometry.

specification were also produced using a regular top drafting roller for comparison purpose. Four yarn bobbins were produced on two spindles from each type of roller. The spindle speed was set at 10,500 rpm, and a ring of 38 mm diameter was used with traveller number 36. The temperature and the relative humidity in the spinning shed were 25 °C and 55%, respectively. The yarn specimens were subjected to yarn quality testing to evaluate yarn hairiness, tensile strength, elongation and yarn evenness. All yarn samples were conditioned for at least 24 h before testing in standard lab conditions (i.e. 20 ± 2 °C temperature and 65 ± 2% relative humidity). Five yarn specimens of 400 m length each were tested for yarn evenness and hairiness on Uster tester 4 (Uster Technologies AG, Uster, Switzerland). Fifty yarn specimens of 500 mm length each were tested for yarn strength and elongation on Uster Tensorapid 4 (Uster Technologies AG, Uster, Switzerland).

Image acquisition

The spinning triangle images were recorded using a Canon 550D (Canon, Japan) high-resolution digital single lens reflex (DSLR) camera, which was coupled with a macro lens (Canon, Japan) of 100 mm focal length. The ISO (light sensitivity of the camera), shutter speed and F-stop number (lens focal length to aperture ratio) of the camera were set to 800, 1/60 and 2.8, respectively. The F-stop number was kept at a minimum to achieve the shallowest possible depth of field to achieve a sharp focus on the spinning triangle. This eradicated any unwanted objects in the images such as fibre fluff and fly by keeping them out of focus. Similarly, the low ISO value was selected to visualize only the main fibrous strand and the spinning triangle and suppress the appearance of any loose fibres surrounding it by assigning them low pixel values in the image. The imaging arrangement is shown in Figure 4. A ruler was placed under the clear rubber roller to calibrate pixel dimensions into physical units (i.e. millimetres). The serial images of the spinning triangle were recorded in a continuous video format at 640 × 480 pixel resolution. Five videos of 30 s each were recorded at 50 frames per second imaging speed and transferred to a computer for image processing.

Digital image processing

An image processing algorithm was developed using various functions from image processing, signal processing and statistical toolboxes in Matlab R2016a (MathWorks, Natick, MA, USA) to process the imagery data of the spinning triangle. The objective of the image processing operations was to quantify the geometrical parameters of the spinning triangle. The steps involved in the image processing are as follows.

- Reading and loading the spinning triangle video into Matlab workspace and splitting it into individual frames (or images).
- Cropping (manually) the spinning triangle in the first image of the sequence using a rectangular drawing tool.
- Using the spatial coordinates of the rectangular region for segmentation of the spinning triangle part from the rest of the image in subsequent frames.
- Adding the pixel intensity values together in each column of the spinning triangle image.
- Smoothing the resultant signal with a Savitzky–Golay algorithm to determine the signal peak, which represented the centre of the fibrous strand.
- Selecting a small rectangular region of 1 mm width at 3 mm distance from the centre of the fibrous strand towards its right to detect roller nip line.
- Applying contrast adjustment and binary conversion to the image to segment roller contact area whose bottom edge represented the roller nip line.
- Extending and drawing the roller nip line 3 mm back into the spinning triangle zone.
- Determining the left and right vertices of the spinning triangle by contrast adjustment and binary conversion of the fibrous strand along the roller nip line.
- Splitting the spinning triangle region into two equal vertical halves to determine third vertex or the tip of the spinning triangle.
- Adding the pixels intensity values in each row as well as in each column in the lower half of the spinning triangle.

- Smoothing the resultant signals through a Savitzky–Golay algorithm to minimize noise fluctuations.
- Detecting the peak of the signal achieved through adding columns, which represented the x-component of the third vertex.
- Detecting the steep decrease in intensity values in the second signal achieved through adding rows, which represented convergence of fibres into the yarn and also the y-component of the third vertex.
- Marking all three vertices on the input spinning triangle image and calculating width, height, left and right angles of the spinning triangle.
- Applying the algorithm on each image in the spinning triangle video and taking an average of measured parameters to represent dynamic geometry of the spinning triangle.

Results and discussion

The clear rubber roller technique was evaluated on three criteria. First, its ability to expose the spinning triangle completely with an acceptable level of clarity was evaluated. Second, the clear rubber roller was investigated for any detrimental effects on the spinning triangle. Finally, the image processing algorithm was applied on a series of spinning triangle images to measure the geometrical parameters and dynamic variations in them.

Completeness and clarity of spinning triangle view

Completeness of spinning triangle image

The primary requirement to measure the geometry of the spinning triangle is to achieve its complete view. A complete picture of the spinning triangle comprises of the area starting from the roller nip line, where a parallel strand of drafted fibres starts to converge under influence of the twisting force (triangle base) down to the yarn twisting point. A typical image of the spinning triangle that was acquired using the clear rubber roller arrangement by the described image acquisition setup is shown in Figure 5(a). The important geometrical features in the spinning triangle image are annotated, as shown in Figure 5(b).

The spinning triangle image taken using the clear rubber roller showed its complete geometry. A continuous parallel strand of fibres (shown within the two purple dotted lines) could be noticed lying on the bottom drafting roller (marked with a red boundary). The fibrous strand then converged into a small triangular shape as it left the roller contact area (marked with a green boundary). The lower boundary of the roller contact area is referred to as the roller nip line, where the fibres started deflecting towards the yarn twisting point (marked with a yellow arrow) under the influence of yarn twist. This deflection of fibres forms the spinning triangle zone (shown with a black boundary), which was only a few millimetres in width and height. The yarn twisting point or the tip of the spinning triangle was exactly the place, where the yarn (marked with a blue arrow) started to form. Hence, the clear rubber roller provided a complete view of the spinning triangle in the images making them suitable for further processing.

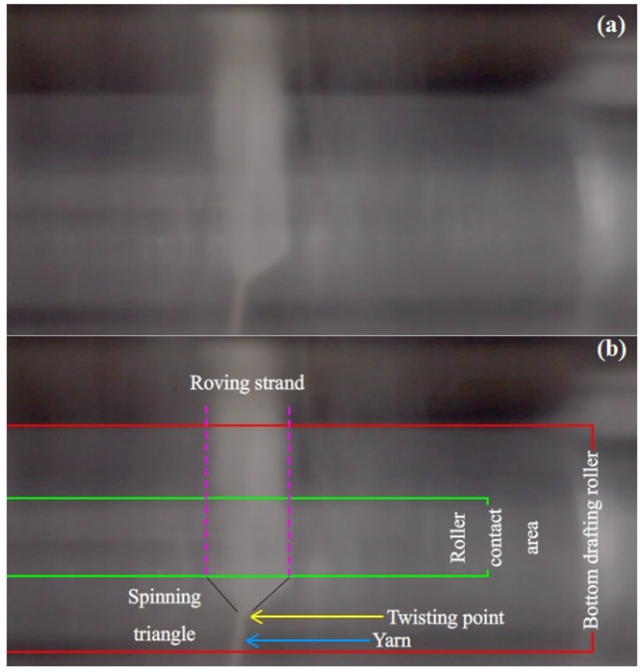

Figure 5. (a) A typical image of the spinning triangle acquired using the clear rubber roller arrangement (b) various areas of interest are annotated.

Clarity of spinning triangle image

In addition to completeness of the spinning triangle image, the second important requirement for further processing was the image quality or clarity to allow recognition and measurement of its geometrical features. The spinning triangle image appeared to be slightly blurred or fuzzy especially near the edges of the fibrous strand. There could be multiple reasons for lack of sharpness in the image such as composite roller structure, fibre accumulation on the roller surface and selection of imaging parameters on the camera. As the clear rubber roller possessed a two-layered composite structure, the light reflecting back from the spinning triangle zone had to pass through two mediums of different refractive indices, i.e. plastic and rubber. These differences in refractive indices could interfere with the reflecting light and the information carried by it causing a deterioration in the image quality. Second, fibres clinging to the roller surface during yarn spinning were noticed. The slight roughness of roller surface along with accumulated residuals of mould release agent made the roller surface slightly sticky causing a few fibres to cling to it. This could also affect the clarity of the roller and the quality of the images taken using it. Finally, the selection of slow shutter speed and low F-stop value to record the rapidly varying spinning triangle and to achieve sharper focus, respectively, were responsible for unavoidable blurriness in the images. However, despite the slight lack of sharpness, the important geometrical features of spinning triangle were recognizable, making the image suitable for further processing.

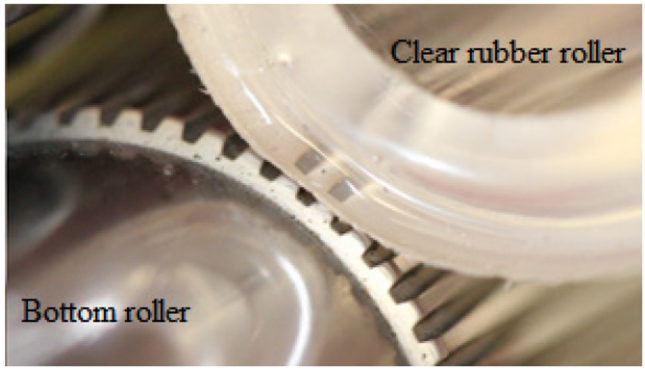

Figure 6. Close-up image of nip formation between bottom steel roller and clear rubber roller.

Non-invasiveness of clear rubber roller

The interfering effects of any measurement system are important to investigate before applying it in a controlled experimental arrangement. The possible interfering effects of the clear rubber roller in regular drafting arrangement could be inadequate nip formation which could be evaluated by a close observation of the nip formation zone. One study suggested fibre slippage at the spinning triangle zone as the key reason for end breakages, a visual observation of fibre slippage in recorded images of the spinning triangle images could reflect the performance of the clear rubber roller (Ghosh, Ishtiaque, Rengasamy, & Patnaik, 2004). Finally, a comparison of quality parameters of yarns produced using a clear rubber roller with the yarns produced using a regular drafting roller would complement the investigation on interfering effects of the clear rubber roller.

Physical observation of nip formation

Figure 6 shows a close-up image of nip formation between the clear rubber roller and the bottom steel roller as the clear rubber roller was mounted in the drafting arm of the ring spinning frame. It can be noticed that the clear rubber roller, due to its flexible surface, slightly deformed upon application of drafting pressure. This resulted in an adequate contact between both rollers leading to an effective nip formation. Such a nip would provide essential control on the fibrous strand during drafting process reducing chances of unwanted fibre slippage at the spinning triangle zone.

Visual observation of fibre slippage

The drafting control on fibres was further investigated by studying a series of spinning triangle images that were recorded using the clear rubber roller during the yarn spinning process. The serial images were taken at 0.5 s interval for a period of 15 s as shown in Figure 7. It can be observed in the image sequence that the shape of the spinning triangle remained consistent and intact as a parallel fibrous strand converged into a yarn under action of the twisting force. Any hint of fibre slippage was not observed in the images, which could cause an end breakage in an extreme case or could at least compromise the basic triangular shape

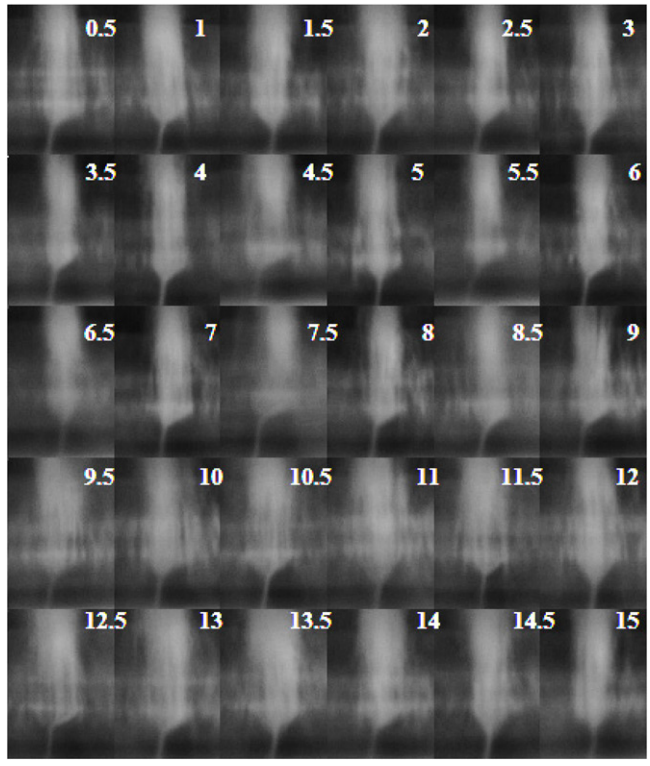

Figure 7. Continuous sequence of the spinning triangle images (contrast adjusted) taken at 0.5 s interval for 15 s.

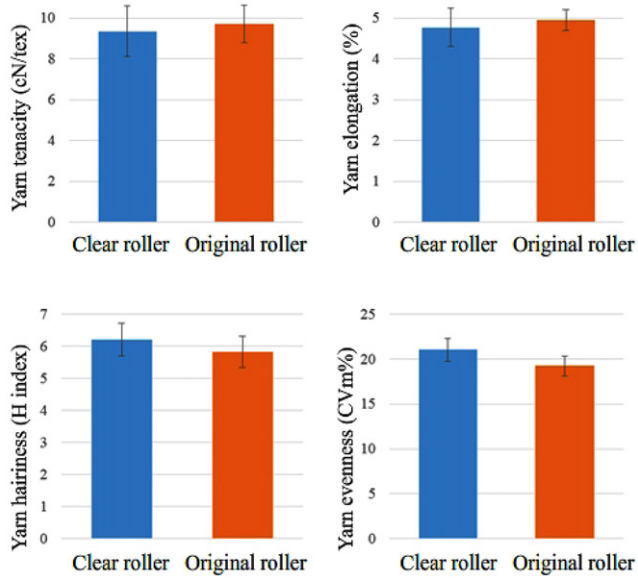

Figure 8. The comparison between the properties of the yarns produced using the clear rubber roller and an original top roller.

of the spinning triangle zone. Hence, it was assumed that a strong and effective control on the fibrous strand by the clear rubber roller was achieved for all experiments.

Comparison of yarn properties

A comparison of the yarns produced using the clear rubber roller and an original drafting roller was made in terms of their physical properties as shown in Figure 8. The differences between the physical properties of the yarns produced

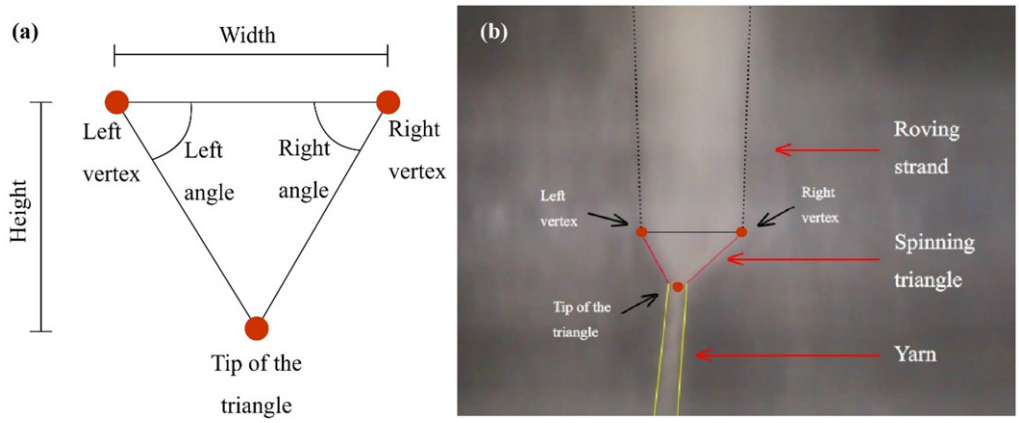

Figure 9. Measurement of the physical geometry of spinning triangle by locating three vertices (a) conceptual illustration (b) applied on a spinning triangle image.

using the clear rubber roller and an original top roller were minute. Although, the yarns produced using the clear rubber roller exhibited slightly less tenacity and elongation than the comparable yarns produced on the original top roller these differences were statistically insignificant (p-values .615 and .482, respectively). Similarly, the slight differences between both yarns in terms of yarn evenness and hairiness were also statistically insignificant (p-values .058 and .257, respectively). As the clear rubber roller did not deteriorate the overall yarn quality significantly, it could be inferred that it did not have a detrimental effect on the actual shape of the spinning triangle.

Measurement of geometrical parameters of the spinning triangle

The recorded images of the spinning triangle were processed using the proposed image processing algorithm to measure parameters such as width, height and angles of the spinning triangle. The principle of measurement is based on locating three vertices of the spinning triangle, as illustrated in Figure 9(a). The horizontal distance between left and right vertices and their vertical distance to the tip of the triangle referred as the width and the height of the triangle, respectively. Similarly, left and right angles of the spinning triangle represent the angles between respective vertex and tip of the triangle. The left and right vertices of the spinning triangle can be located if the roller nip line can be determined in the spinning triangle image. The fibres start converging into a triangular shape at roller nip line and both left and right vertices lie on it at respective sides of the fibrous strand. The third vertex is essentially the yarn twisting point, which lies at the tip of the triangle as shown in Figure 9(b). The image processing algorithm located three vertices of the spinning triangle in each image of the recorded video leading to measurement of its important geometrical parameters and variations in them over time.

Application of image processing algorithm

An example of applying the image processing algorithm on one spinning triangle image and its outcomes are demonstrated in Figure 10. The first image of the spinning triangle video sequence was cropped by the user to manually select the spinning triangle region using a rectangle drawing tool as shown in Figure 10(a). This isolated the area of interest in the image for application of the image processing operations. Two of the important requirements of quantifying the spinning triangle geometry were determining the roller nip line and the yarn twisting point as the left and right vertices lay on the roller nip line while the third vertex lay on its tip. The roller nip line could be determined anywhere along the width of the bottom drafting roller. However, the ideal place was where the presence of fibre fluff and fly was at a minimum, i.e. at some distance from the main fibrous strand. The centre of the fibrous strand needed to be nominated before drawing a nip line so that it could be used as a reference. To achieve this, the sum of all pixel values (i.e. greyscale intensity) in each column of the selected rectangular region was calculated and plotted in Figure 10(b). The Savitzky–Golay algorithm was applied on the resulting signal for smoothing it as shown in Figure 10(c). The peak of the signal represented the centre of the fibrous strand as the maximum number of non zero pixels (white fibre pixels) lay in the column that formed the centre of the fibrous strand. The detected centre of the triangle was imposed on the initial image in a green color as shown in Figure 10(d).

Further proceeding with determination of the roller nip line, a small 1 mm wide region was selected at 3 mm right offset to the centre of the fibrous strand as shown in Figure 10(e). The selected area being quite distant from the spinning triangle zone had minimal chance of the presence of fibre fluff or fly that could possibly affect the roller nip detection. The principle of determining the roller nip line was based on the fact that the maximum reflection of light occurred at the contact area of the clear rubber roller and bottom steel roller producing a relatively brighter region in the image. This bright region was detected by basic contrast adjustment and binary conversion of the image as shown in a small window in Figure 10(e). The bottom row of the pixels of the roller contact area represented the roller nip line, which was then extended back to the spinning triangle zone as illustrated in Figure 10(f). As the left and right vertices of the triangle lay on the roller nip line, they were determined by simple thresholding of the light coloured fibrous strand from the darker background.

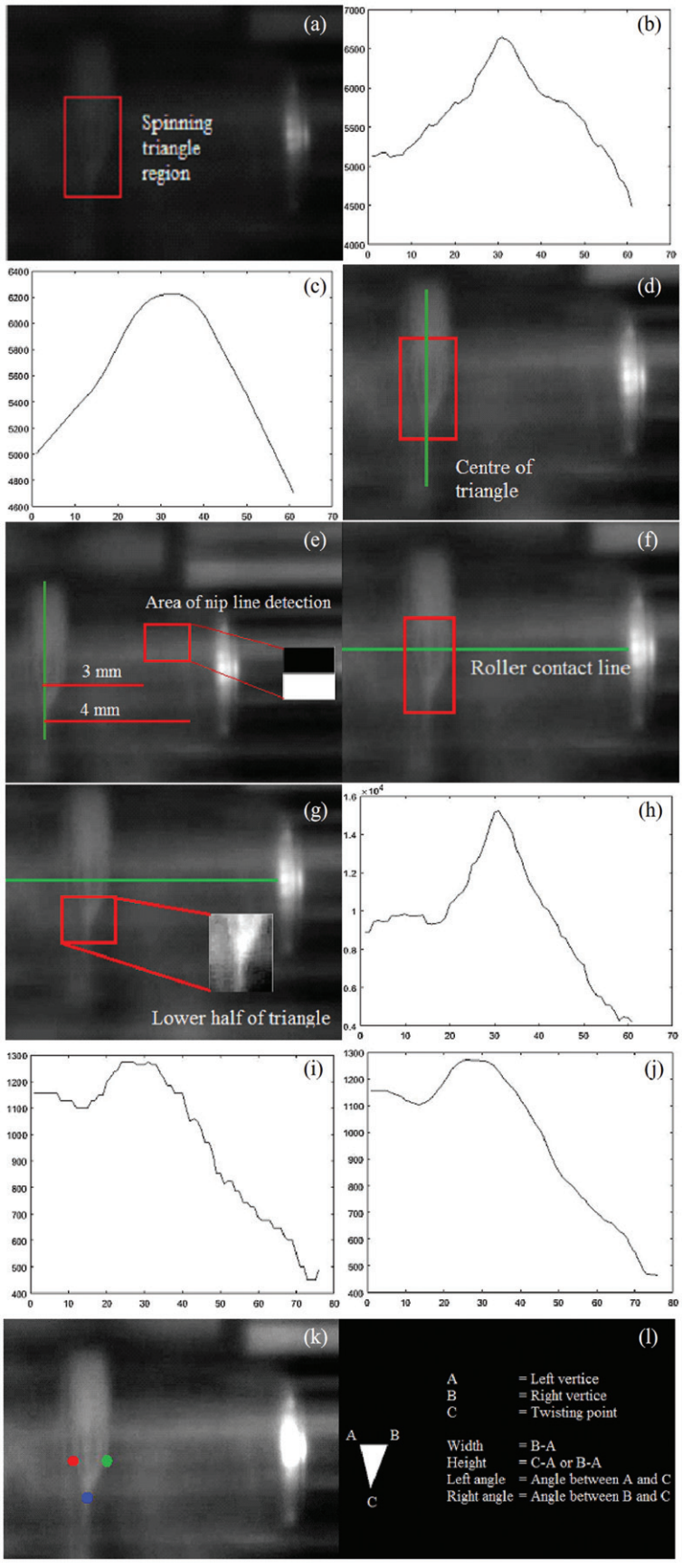

Figure 10. Various stages in processing of the spinning triangle images: (a) cropping the spinning triangle region by user, (b) taking sum of the columns of the selected region, (c) applying Savitzky–Golay smoothing filter, (d) determining the centre of the fibrous strand, (e) determination of roller contact line by selecting an area at 3–4 mm distance from the spinning triangle, (f) mapping of the roller nip line on the image, (g) selecting the lower half of the spinning triangle zone, (h) taking the sum of the columns of selected area to locate yarn centre, (i) taking the sum of rows of selected area, (j) application of the Savitzky–Golay smoothing filter to detect a steep decrease in pixel intensity at the yarn twisting point, (k) plotting three vertices of the triangle, (l) simulation of the spinning triangle geometry with measurement of its geometrical parameters.

To locate the third vertex of the spinning triangle, the rectangular region as shown in Figure 10(a) was split into two equal vertical halves, i.e. top triangle zone and the bottom triangle zone. The yarn twisting point essentially lay in the bottom half of the spinning triangle as shown in Figure 10(g). The yarn twist point was the specific point, where the triangular shape spread of fibres converged into a yarn. The pixels in each column and row of the bottom half of the spinning triangle zone were added seperately and plotted as shown in Figure 10(h) and (i), respectively. The signal plotted in Figure 10(i) was smoothed using Savitzky–Golay filter as shown in Figure 10(j) to minimize unwanted noise and fluctuations. The peak of the signal in Figure 10(h) referred to the yarn centre while a sharp decrease in Figure 10(j) referred to the area where the triangle converged into a yarn. Both of these points were taken as horizontal (x) and vertical (y) coordinates of the yarn twisting point, respectively. The yarn twisting point was then marked on the actual spinning triangle image as shown in Figure 10(k). Various measurements regarding the spinning triangle geometry were conducted through these three coordiantes as shown in Figure 10(l). The image processing algorithm was looped over a sequence of 500 serial images and averaged values of the geometrical parameters are given in Figure 11 along with simulated representation of the spinning triangle geometry. It is also important to note that a slight chance of error in the measurements could not be neglected due to presence of unavoidable frayed fibres surrounding the actual spinning triangle zone.

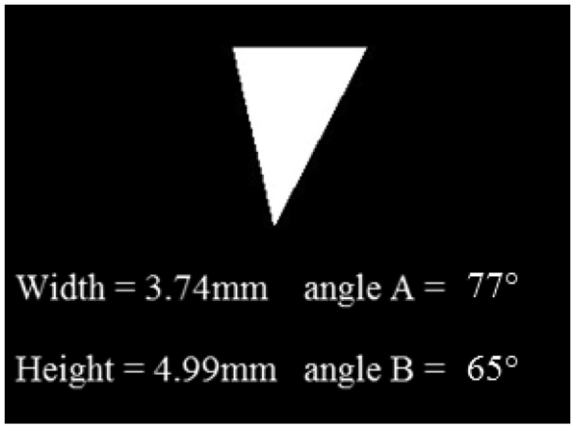

Figure 11. Measurement of geometrical parameters of spinning triangle (20 tex yarn) using digital image processing algorithm.

Analysing dynamic behaviour of the spinning triangle geometry

In order to study the dynamic nature of the spinning triangle geometry, its geometrical parameters were plotted in the time and the frequency domains (by applying Fourier transformation) as shown in Figures 12–15. A significant amount of variation could be noticed in all four geometrical parameters of the spinning triangle with respect to time. The width of the spinning triangle has a relationship with the evenness of the roving strand as it expands and contracts due to the presence of thick and thin places, respectively (Badehnoush & Alamdar-Yazdi, 2011). The low magnitude random irregularities in the width signal could be linked to the natural variations in the fibre material and the intrinsic variations in the spinning process as shown in Figure 12(a). In addition, a roving strand might contain periodic faults caused by factors such as roller eccentricity.

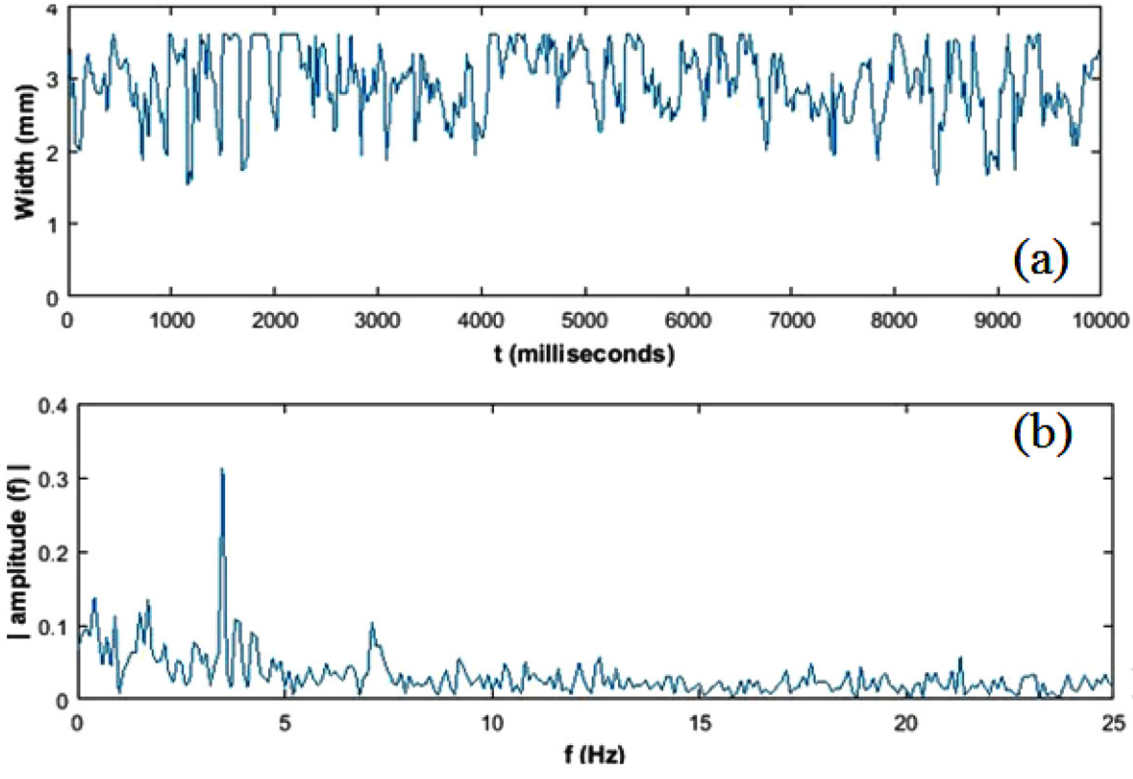

Figure 12. Variations in the width of the spinning triangle in (a) time domain (b) frequency domain.

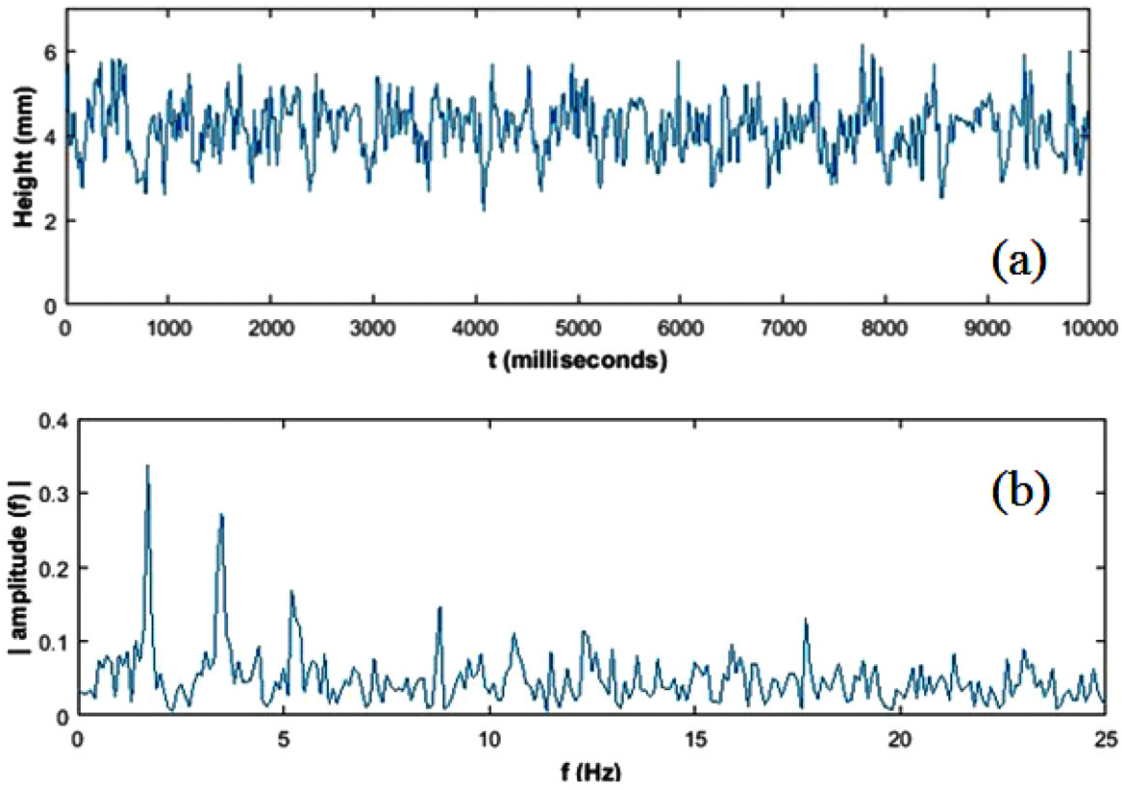

Figure 13. Variation in the height of the spinning triangle in (a) time domain (b) frequency domain.

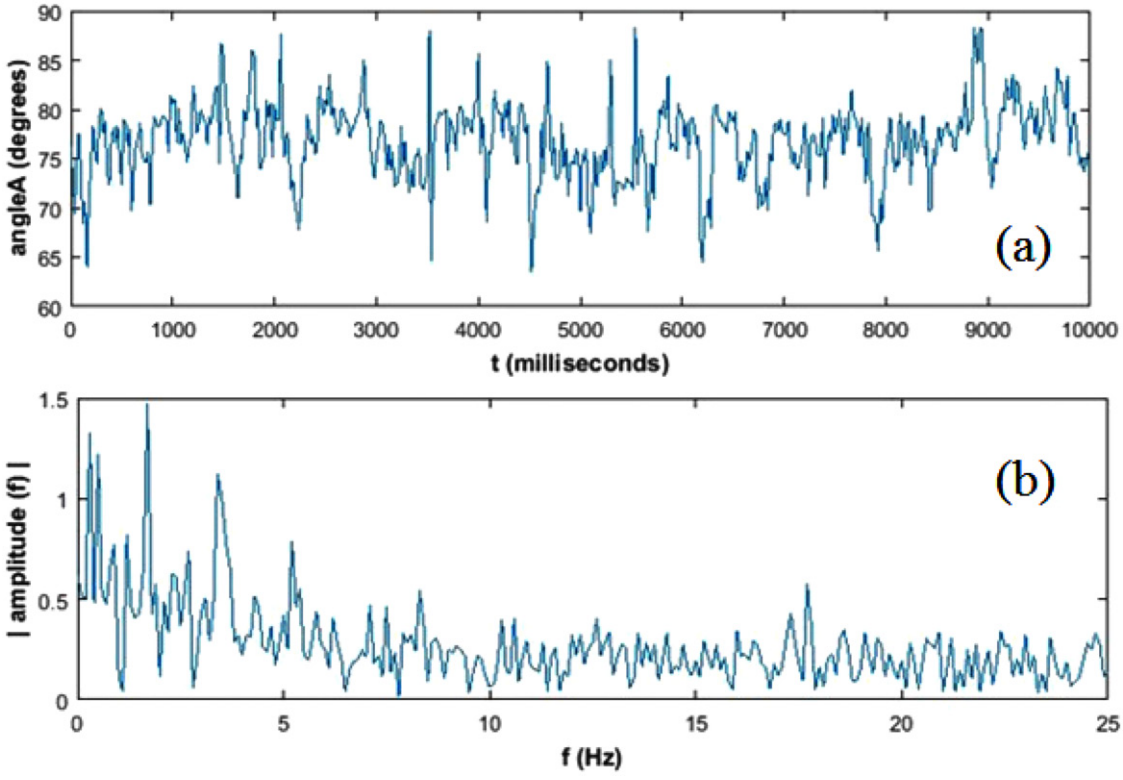

Figure 14. Variation in the angle A (left angle) of the spinning triangle in (a) time domain (b) frequency domain.

These periodic variations could only be exposed in frequency domain. For example, a 4-Hz peak could be noticed in the Fourier plot given in Figure 12(b), which may be referring to a periodic fault in the roving strand.

The trend of the variation in height of the spinning triangle appeared to follow an oscillatory pattern as shown in Figure 13(a). These variations might be linked to the yarn formation and twisting process (Hua, Tao, Cheng, & Xu,

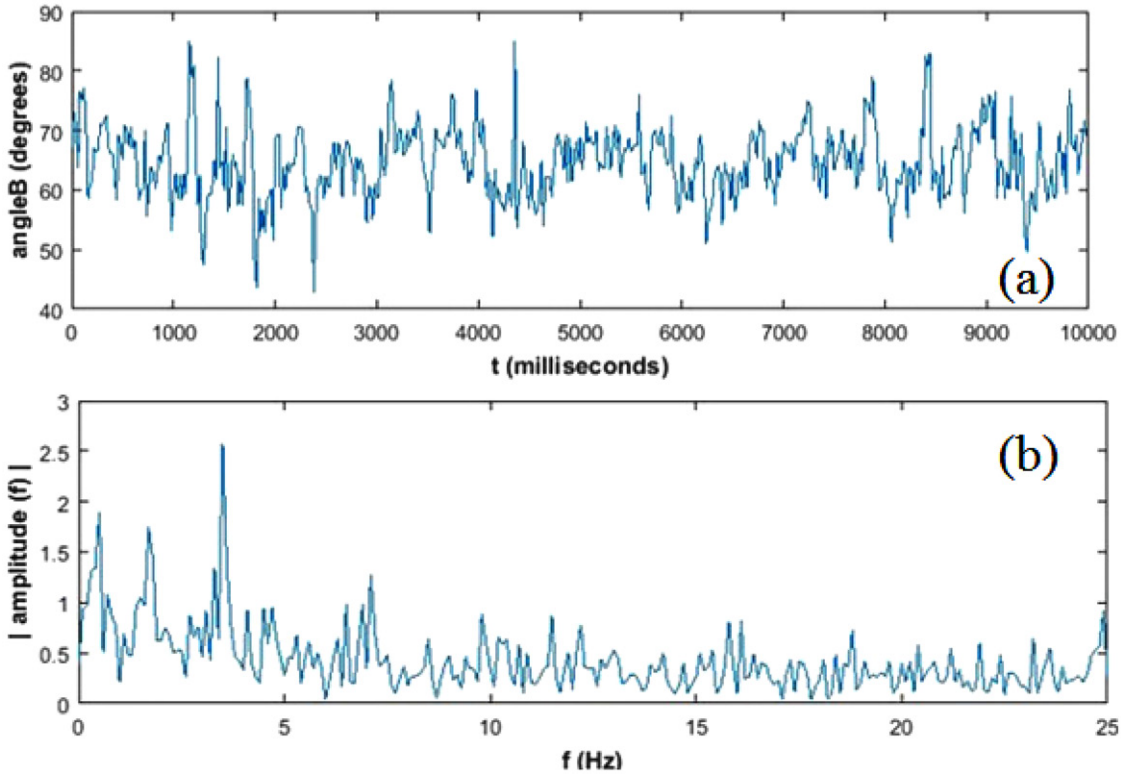

Figure 15. Variation in the angle B (right angle) of the spinning triangle in (a) time domain (b) frequency domain.

2007). The height of the spinning triangle decreased and increased subsequently due to fibre twisting and inward motion of the roving strand into the spinning triangle zone, respectively, generating a repetitive pattern of alternative peaks and valleys. The Fourier transformation of the height signal showed the maximum amplitude peak at around 2 Hz frequency as shown in Figure 13(b). This coincides with the number of twists inserted into the spinning triangle zone in 1 s, i.e. 2.18 twists per second (at 798 TPM and 10,500 rpm spindle speed). Hence, the periodic variations in the height of the spinning triangle could be attributed to yarn formation and twisting process.

Both angles of the spinning triangle showed some degree of oscillation in their magnitudes as shown in Figure 14(a) and Figure 15(a). However, this variation appeared to be quite random due to the presence of multiple peaks in the respective frequency spectrums as shown in Figure 14(b) and Figure 15(b).

Conclusions

A new method based on the combination of a clear rubber roller and digital image processing techniques was developed to measure the geometry of the spinning triangle during ring spinning. The clear rubber roller revealed the spinning triangle by exposing its complete geometry with an acceptable level of clarity. The clear rubber roller did not significantly influence the fibre arrangement in the spinning triangle zone or its classical shape as observed by physical analysis of the nip formation zone and visual analysis of the spinning triangle image sequence. In addition, the comparison of the yarns produced on the clear rubber roller and the regular drafting roller did not show statistically significant differences in key yarn properties, indicating normal operation of the clear rubber roller. The spinning triangle images were processed using the image processing algorithm in an automated manner and its geometrical parameters such as width, height and angles were measured across the image dataset. The dynamic analysis of the geometrical parameters of the spinning triangle showed continuous fluctuations under the influence of material and process related variables. The analysis of geometrical parameters in frequency domain revealed that the variations in the width and the height of the spinning triangle were caused by natural variations in the roving strand and twist propogation in the spinning triangle zone, respectively. In the second part of this study, this combined method will be applied in controlled yarn production arrangement to study the geometry and dynamics of the spinning triangle and its effect on resultant yarn quality.

Disclosure statement

No potential conflict of interests was reported by the authors.

Funding

This work was partially supported by the Australian Research Council (ARC) through a Linkage project (LP120200536)

References

Altas, S., & Kadoğlu, H. (2012). Comparison of conventional ring, mechanical compact and pneumatic compact yarn spinning systems. *Journal of Engineered Fibers and Fabrics*, *7*(1), 87–100.

Badehnoush, A., & Alamdar-Yazdi, A. (2011). Real-time yarn evenness investigation via evaluating spinning triangle area changes. *The Journal of the Textile Institute*, *103*(8), 850–861.

Basal, G., & Oxenham, W. (2006). Comparison of properties and structures of compact and conventional spun yarns. *Textile Research Journal*, *76*(7), 567–575.

Feng, J., Xu, B., Tao, X., & Hua, T. (2010). Theoretical study of a spinning triangle with its application in a modified ring spinning system. *Textile Research Journal*, *80*(14), 1456–1464.

Ghosh, A., Ishtiaque, S., Rengasamy, S., & Patnaik, A. (2004). The mechanism of end breakage in ring spinning: A statistical model to predict the end break in ring spinning. *Autex Research Journal*, *4*(1), 19–24.

Hua, T., Tao, X. M., Cheng, K. P. S., & Xu, B. G. (2007). Effects of geometry of ring spinning triangle on yarn torque part I: Analysis of fiber tension distribution. *Textile Research Journal*, *77*(11), 853–863.

Kennedy, J. B., & Neville, A. M. (1986). *Basic statistical methods for engineers and scientists*. New York, NY: Harper & Row.

Klein, W. (2008). *The Rieter manual of spinning: Technology of short-staple spinning*. Winterthur, Switzerland: Rieter.

Lawrence, C. A. (2010). *Advances in yarn spinning technology*. Derbyshire, UK: Woodhead.

Lord, P. R., & Grover, G. (1993). Roller drafting. *Textile Progress*, *23*(4), 5–8.

Mahdiyeh, D., & Esfandiyar, E. (2014). Review of distribution of fiber tension at the spinning triangle. *The Journal of the Textile Institute*, *105*(11), 1167–1177.

Najar, S. (1996). An analysis of the twist triangle in ring spinning (Doctoral dissertation). University of New South Wales, NSW, Australia.

Sears, F. W., Zemansky, M. W., & Young, H. D. (1976). *University physics*. Boston, USA: Addison-Wesley.

Thilagavathi, G., Udayakumar, D., Sasikala, L., & Kannaian, T. (2009). Yarn hairiness controlled by various left diagonal yarn path offsets by modified bottom roller flute blocks in ring spinning. *Indian Journal of Fibre and Textile Research*, *34*(4), 328–332.

Tyagi, G. K., Bhowmick, M., Bhattacharyya, S., & Kumar, R. (2010). Effect of spinning conditions on mechanical and performance characteristics of cotton ring- and compact-spun yarns. *Indian Journal of Fibre and Textile Research*, *35*(1), 21–30.

Wang, X., & Chang, L. (2003). Reducing yarn hairiness with a modified yam path in worsted ring spinning. *Textile Research Journal*, *73*(4), 327–332.

Wang, X., Huang, W., & Huang, X. B. (1999). A study on the formation of yarn hairiness. *Journal of the Textile Institute*, *90*(1), 555–569.

Wei, L., Huang, S., Zhu, T., & Su, X. (2015). Research on shape of spinning triangles in the ring spinning system. *The Journal of the Textile Institute*, *107*(4), 420–430.

Xia, Z., & Xu, W. (2013). A review of ring staple yarn spinning method development and its trend prediction. *Journal of Natural Fibers*, *10*(1), 62–81.